

Deterministic and scalable generation of large Fock states

Mo Xiong,^{1,*} Jize Han,^{2,*} Chuanzhen Cao,¹ Jinbin Li,^{1,3} Qi Liu,^{4,†} Zhiguo Huang,^{2,‡} and Ming Xue^{1,3,§}

¹*Department of Physics, Nanjing University of Aeronautics and Astronautics, Nanjing 211106, China.*

²*China Mobile (Suzhou) Software Technology Co., Ltd., Suzhou, 215163, China*

³*Center for the Cross-disciplinary Research of Space Science and Quantum-technologies (CROSS-Q), Nanjing 211106, China.*

⁴*National Laboratory of Solid State Microstructures and School of Physics,*

Collaborative Innovation Center of Advanced Microstructures,

Nanjing University, Nanjing 210093, People's Republic of China

(Dated: January 16, 2026)

The scalable and deterministic preparation of large Fock-number states represents a long-standing frontier in quantum science, with direct implications for quantum metrology, communication, and simulation. Despite significant progress in small-scale implementations, extending such state generation to large excitation numbers while maintaining high fidelity remains a formidable challenge. Here, we present a scalable protocol for generating large Fock states with fidelities exceeding 0.9 up to photon numbers on the order of 100, achieved using only native control operations and, when desired, further enhanced by an optional post-selection step. Our method employs a hybrid Genetic-Adam optimization framework that combines the global search efficiency of genetic algorithms with the adaptive convergence of Adam to optimize multi-pulse control sequences comprising Jaynes-Cummings interactions and displacement operations, both of which are native to leading experimental platforms. The resulting control protocols achieve high fidelities with shallow circuit depths and strong robustness against parameter variations. These results establish an efficient and scalable pathway toward high-fidelity non-classical state generation for precision metrology and fault-tolerant quantum technologies.

I. INTRODUCTION

The ability to deterministically prepare highly nonclassical bosonic states is a central goal in quantum science, with far-reaching implications for quantum metrology, communication, simulation, and fault-tolerant quantum technologies [1–11]. Among these states, Fock states $|N\rangle$ —energy eigenstates with a precisely defined number of excitations—constitute fundamental non-Gaussian resources [12–14]. As the excitation number increases, large- N Fock states exhibit increasingly fine phase-space interference and enhanced sensitivity to external perturbations, thereby enabling superior performance in precision sensing [15, 16] and bosonic quantum information protocols [17, 18]. At the same time, these very properties render their scalable and deterministic preparation particularly challenging.

Over the past decades, remarkable progress has been achieved in generating single- and few-excitation Fock states across a wide range of experimental platforms [19–26]. However, extending such capabilities to large Fock numbers remains elusive [27–38]. Most existing approaches rely on probabilistic processes, including measurement-based filtering [16, 39, 40], or exploit bosonic nonlinearities [41–44], or dissipation engineering [45]. Deterministic schemes based on sequential population transfer or photon-number subtraction or addition [21, 34, 46–48], on the other hand, require an increasing number of elementary operations as N grows, leading to rapid accumulation of control errors and decoherence. Despite their effectiveness at small scales, all these ap-

proaches are ultimately constrained by fundamental trade-offs between determinism, robustness, and scalability.

From a broader control perspective, these difficulties reflect an inherent trade-off between available control resources and the complexity of the required control protocols, which becomes increasingly restrictive as the target Fock number grows. These challenges point to a more general obstacle: the difficulty of engineering strong and well-controlled photon-number-dependent phases across a large bosonic Hilbert space [49–51]. Despite important advances, achieving deterministic, scalable, and high-fidelity preparation of large- N Fock states remains an open problem, and continued exploration of diverse and complementary approaches is both necessary and valuable.

Here we formulate large-Fock-state preparation as a task of engineering interference through time-structured, photon-number-dependent dynamics, rather than relying on sequential population transfer or bosonic nonlinearities. This perspective reframes the problem from population engineering to coherent interference engineering in Fock space. Our approach exploits the intrinsic nonlinear spectrum of the Jaynes-Cummings interaction, which naturally generates photon-number-dependent phase accumulation while remaining natively available across a wide range of experimental platforms, including cavity and circuit QED [52, 53], trapped ions [54, 55], and other AMO systems [56]. By combining Jaynes-Cummings interactions with phase-space displacement operations, we construct composite control sequences that deterministically reshape an initial coherent-state distribution through engineered interference in Fock space.

We demonstrate the generation of large Fock states with fidelities exceeding 0.9 up to $N \gtrsim 100$, with success probabilities close to unity upon optional post-selection. The resulting protocols employ only native spin-oscillator operations, require shallow control depths, and exhibit robustness

* These authors contributed equally to this work.

† louisliu9267@gmail.com

‡ huangzhiguo15@mails.ucas.ac.cn

§ mxue@nuaa.edu.cn

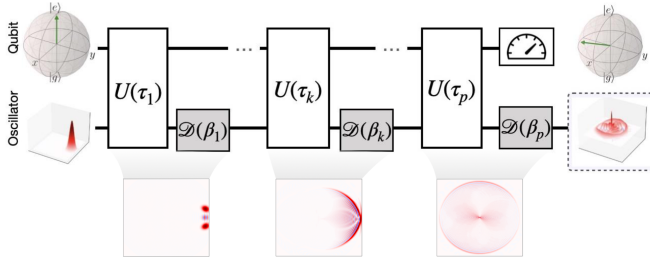


Figure 1. Multi-pulse Jaynes–Cummings–displacement protocol for Fock-state generation. The control sequence consists of p layers, each comprising a resonant Jaynes–Cummings evolution $U(\tau_k)$ acting on the joint qubit–oscillator system, followed by a phase-space displacement $D(\beta_k)$ applied to the bosonic mode. The qubit is initialized in the excited state and the oscillator in a coherent state. Repeated accumulation of photon-number–dependent phases arising from the nonlinear Jaynes–Cummings spectrum, combined with displacement-induced interference, progressively reshapes the oscillator state in phase space. The second row shows representative Wigner-function snapshots at different layers of the protocol, illustrating the emergence of nonclassical interference fringes characteristic of high-number Fock states. A final projective measurement on the qubit can be used to disentangle the qubit from the oscillator.

against detuning, control noise, and experimentally relevant dissipation. Our results establish a scalable and experimentally accessible route toward high-fidelity Fock-state generation, opening new opportunities for quantum-enhanced sensing and bosonic quantum technologies.

II. RESULTS

A. Composite-pulse protocol.

We consider a spin–boson interaction in which a two-level system couples to a single-mode quantized field. This standard setting—described by the Jaynes–Cummings (JC) Hamiltonian—captures the essential physics of light–matter interaction across cavity QED, circuit QED, and related platforms. In the rotating frame ($\hbar = 1$), the Hamiltonian reads

$$\hat{H} = -\Delta \hat{a}^\dagger \hat{a} + \Omega (\hat{a} \hat{\sigma}_+ + \hat{a}^\dagger \hat{\sigma}_-), \quad (1)$$

where $\Delta = \omega_q - \omega_c$ denotes the detuning between the qubit and cavity frequencies ($\Delta = 0$ hereafter for the resonant case), and Ω is the coupling strength. The operators \hat{a} (\hat{a}^\dagger) annihilate (create) photons in the cavity mode, while $\hat{\sigma}_-$ ($\hat{\sigma}_+$) $= |g\rangle\langle e|$ ($|e\rangle\langle g|$) lower (raise) the qubit between its ground and excited states $|g\rangle$ and $|e\rangle$.

Our objective is to prepare a target Fock state $\rho_N = |N\rangle\langle N|$ of the bosonic mode. The protocol begins with the cavity initialized in a coherent state $|\alpha\rangle$ of mean photon number $|\alpha|^2 = N$, which provides a physically natural and experimentally accessible seed for Fock-state synthesis. The full initial state is therefore $|\Psi_0\rangle = |e\rangle|\alpha\rangle$.

As depicted in Fig. 1, the control sequence consists of p composite pulses alternating between JC evolution and

phase-space displacement operations. The sequence is fully specified by $\{\tau, \beta\}$, where $\tau = (\tau_1, \dots, \tau_p)$ and $\beta = (\beta_1, \dots, \beta_p)$. After the full sequence, the joint atom-field state is

$$|\Psi(\tau, \beta)\rangle = \left[\prod_{k=1}^p \hat{D}(\beta_k) \hat{U}(\tau_k) \right] |\Psi_0\rangle, \quad (2)$$

where $\hat{U}(\tau_k) = e^{-i\hat{H}\tau_k}$ is JC evolution of duration $\tau_k \in \mathbb{R}^+$, and $\hat{D}(\beta_k) = e^{\beta_k \hat{a}^\dagger - \beta_k \hat{a}}$ displaces the field by amplitude $\beta_k \in \mathbb{C}$.

A key structural feature of the protocol is the time-control index (l), which specifies the total evolution time through its relation to the JC quantum revival structure [57]:

$$\Omega T_R^{(l)} \approx (2l + 1)\pi\sqrt{N}.$$

For a single-layer circuit ($p = 1$), the protocol connects directly to the operation of Ref. [37]. In the multi-pulse setting, however, the interplay between multiple JC segments and displacement operations generates a much richer interference landscape. As a result, the optimized solutions obtained variationally typically employ a total evolution time shorter than the single-pulse revival time for the same target N . Accordingly, the control parameters are defined under the global timing scale set by $T_R^{(l)}$, while leaving the internal pulse structure unconstrained.

The cavity state resulting from this sequence may be obtained directly by tracing out the qubit, or, alternatively, via a projective measurement on the qubit (cf. Fig. 1). In the latter case, the qubit is projected onto $|\psi_q\rangle = \cos(\varphi_0/2)|g\rangle + \sin(\varphi_0/2)e^{i\varphi_1}|e\rangle$ with $\varphi = \{\varphi_0, \varphi_1\}$, which removes the remaining atom–field correlations and yields a purer cavity state. This optional post-selection step removes the residual qubit–field correlations and yields a purer cavity state, with a success probability close to unity.

High-fidelity preparation is obtained by optimizing over the $3p + 2$ control parameters

$$\boldsymbol{\theta} = \{\tau, \beta, \varphi\}. \quad (3)$$

The quality of the prepared cavity state ρ_θ is characterized by its Uhlmann–Jozsa fidelity with the target Fock state ρ_N ,

$$\mathcal{F}(\boldsymbol{\theta}) = \left(\text{Tr} \sqrt{\sqrt{\rho_\theta} \rho_N \sqrt{\rho_\theta}} \right)^2. \quad (4)$$

To avoid repeated reduced-state evaluations during optimization, we instead minimize the proxy loss

$$\mathcal{L}_\theta = 1 - |\langle \Psi(\tau, \beta) | \Psi_N(\varphi) \rangle|^2, \quad (5)$$

where $|\Psi_N\rangle = |\psi_q(\varphi)\rangle \otimes |N\rangle$ denotes the ideal disentangled target state. This variational formulation enables efficient optimization of multi-pulse controls and naturally generalizes the single-pulse JC approach to a richer, more flexible control landscape that attains higher fidelity at significantly shorter evolution times.

Algorithm 1 GAdam hybrid optimization

Input: Target photon number N ; revival index l ; number of layers p ; loss function $\mathcal{L}(\theta)$; population size P ; elite size E ; number of generations G ; tournament size s ; crossover rate r_c ; mutation scale r_m ; Adam pre-optimization steps S_{pre} ; final Adam refinement steps S_{fin} ; minimum pulse duration τ_{\min} ; displacement bound β_{\max} ; time-mismatch tolerance ϵ_T .
Output: Optimized parameters $\theta^* = \{\tau^*, \beta^*, \varphi^*\}$.

- 1: **Initialization from single-layer seed**
 Load optimized $p=1$ solution $\theta_1^{\text{opt}} = \{\tau_1^{\text{opt}}, \beta_1^{\text{opt}}, \varphi^{\text{opt}}\}$ for the same (N, l) .
 Set global target time $T_{\text{tar}} \leftarrow \tau_1^{\text{opt}}$ (or $T_R^{(l)}$ if specified).
for $i = 1, \dots, P$
 $\varphi^{(i)} \leftarrow \varphi^{\text{opt}}$, $\beta_p^{(i)} \leftarrow \beta_1^{\text{opt}}$, and $\beta_k^{(i)} \leftarrow 0$ for $k = 1, \dots, p-1$.
 Sample $\{\tau_k^{(i)}\}_{k=1}^p$ such that $\sum_{k=1}^p \tau_k^{(i)} = T_{\text{tar}}$ and $\tau_k^{(i)} \geq \tau_{\min}$.
end for
- 2: **Hybrid genetic and Adam**
for $g = 1, \dots, G$
 Adam pre-optimization
 for $i = 1, \dots, P$
 $\theta^{(i)} \leftarrow \text{Adam}(\theta^{(i)}, \mathcal{L}, S_{\text{pre}})$.
 Enforce bounds: $\tau_k^{(i)} \geq \tau_{\min}$, $|\beta_k^{(i)}| \leq \beta_{\max}$.
 end for
 Compute fitness $f^{(i)} = 1 - \mathcal{L}(\theta^{(i)})$
 Select elite set $\mathcal{P}_{\text{elite}}$ of top- E individuals.
 Genetic reproduction
 $\mathcal{P}_{\text{off}} \leftarrow \emptyset$
 while $|\mathcal{P}_{\text{off}}| < P - E$
 Select parents by tournament selection: $\theta^{(A)}, \theta^{(B)}$.
 Apply uniform crossover with probability r_c .
 Apply Gaussian mutation: $\theta^{\text{child}} \leftarrow \theta^{\text{child}} + \mathcal{N}(0, r_m^2)$.
 Enforce bounds: $\tau_k \geq \tau_{\min}$, $|\beta_k| \leq \beta_{\max}$.
 Soft time constraint: rescale $\tau_k \rightarrow \tau_k T_{\text{tar}} / \sum_j \tau_j$
 if $|\sum_k \tau_k - T_{\text{tar}}| / T_{\text{tar}} > \epsilon_T$.
 Add θ^{child} to \mathcal{P}_{off} .
 end while
 Update population: $\mathcal{P} \leftarrow \mathcal{P}_{\text{elite}} \cup \mathcal{P}_{\text{off}}$.
end for
 $\theta^* \leftarrow \arg \min_{\theta \in \mathcal{P}} \mathcal{L}(\theta)$.
- 3: **Adam refinement**
 $\theta^* \leftarrow \text{Adam}(\theta^*, \mathcal{L}, S_{\text{fin}})$. =0

B. GAdam optimization framework.

Optimizing the $3p + 2$ control parameters in Eq. 3 requires navigating a highly non-convex landscape with many periodic local minima (See Methods). To efficiently explore this landscape and obtain high-fidelity solutions, we employ a hybrid genetic–Adam (GAdam) optimization strategy, summarized in Algorithm Box, which combines global stochastic search with local gradient-based refinement.

Transfer initialization. As described in Step 1 of Algorithm Box, the optimization is seeded by a transfer-initialization procedure based on an optimized single-layer ($p = 1$) solution at the same target photon number N and revival index l . The optimized parameters $\theta_1^{\text{opt}} = \{\tau_1^{\text{opt}}, \beta_1^{\text{opt}}, \varphi^{\text{opt}}\}$ define a physically meaningful global timing scale. This total evolution time, denoted T_{tar} , is fixed either to τ_1^{opt} or to the revival-based estimate $T_R^{(l)}$. Initial multi-

pulse candidates are generated by randomly partitioning T_{tar} into p segments $\{\tau_k\}$ subject to $\tau_k \geq \tau_{\min}$, while inheriting the optimized final displacement β_p^{opt} and qubit measurement basis φ^{opt} . All intermediate displacements are initialized to zero. This construction places the initial population close to a physically relevant manifold, avoiding inefficient exploration of low-fidelity regions.

Hybrid genetic and Adam search. The optimization then proceeds iteratively over G generations (Step 2 of Algorithm Box). Within each generation, every individual first undergoes a short Adam pre-optimization using the loss function $\mathcal{L}(\theta)$, which introduces diversity and improves the overall population quality before genetic selection. After enforcing hard bounds on pulse durations and displacement amplitudes, the fitness of each individual is evaluated as $f = 1 - \mathcal{L}(\theta)$. An elite subset of the top- E individuals is retained unchanged.

New candidates are generated through tournament-based parent selection, uniform crossover of control parameters, and Gaussian mutation. A soft global timing constraint is imposed: if the total duration deviates from T_{tar} beyond a relative tolerance ϵ_T , all τ_k are rescaled proportionally to restore the target total time. This allows the optimizer to freely redistribute pulse durations while preserving the global interference timescale set by the JC revival structure. The next generation is formed by combining the elite set with the newly generated offspring.

Final refinement. After G generations, the individual with the minimal loss is selected and subjected to a final, high-precision Adam refinement (Step 3 of Algorithm Box). The resulting parameters $\theta^* = \{\tau^*, \beta^*, \varphi^*\}$ define the optimized composite-pulse sequence used in the performance and robustness analyses.

C. Fidelity and dynamics.

Figure 2 summarizes the performance of the multi-pulse protocol and reveals the dynamical mechanism underlying high-fidelity Fock-state synthesis. The fidelities in Fig. 2(a) show that the protocol maintains $\mathcal{F} \gtrsim 0.90$ for $N \gtrsim 100$. Representative circuit depths with $p = 1, 2, 6, 10$ layers highlight the expected trend: shallow circuits already outperform the single-pulse baseline, while deeper circuits sustain high fidelities for larger photon numbers. Since the optimized index l grows only weakly with N , the total evolution time $T_N \propto l\sqrt{N}$ scales sublinearly with the target photon number. The post-selection success probability remains high across all N and circuit depths, with $P_{\text{succ}} \gtrsim 0.9$ throughout the explored parameter range [Fig. 2(b)]. This confirms that the qubit projection acts primarily as a disentangling step, yielding a purer photonic state without compromising near-deterministic operation.

The evolution of the photon-number distribution is illustrated in Fig. 2(c) for the case $N = 100$ under a nine-pulse sequence, where four representative layers (1, 4, 6, and 9) are shown. The alternating JC evolution and displacement operations progressively reshape the initial Poissonian population into an increasingly symmetric pattern centered at $n = 100$.

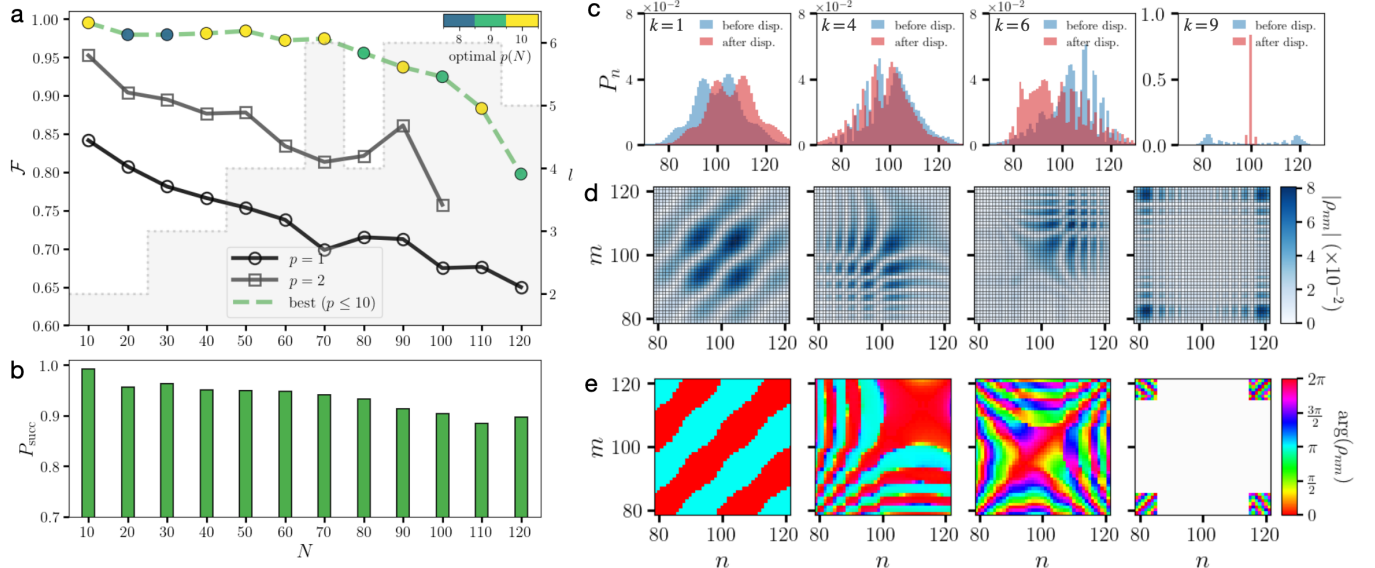


Figure 2. Performance and internal dynamics of the multi-pulse Jaynes–Cummings–displacement protocol. (a) Fidelity \mathcal{F}_N as a function of the target photon number N . Black circles and gray squares show results obtained with fixed circuit depths $p = 1$ and $p = 2$, respectively. Colored markers connected by the dashed green line indicate the best fidelity achieved for each N among circuits with depths up to $p \leq 10$, with the corresponding optimal depth $p(N)$ encoded by color. The data demonstrate that shallow multi-pulse circuits substantially outperform single-pulse protocols and sustain high fidelities up to $N \gtrsim 100$. (b) Post-selection success probability P_{succ} corresponding to the optimal protocols shown in panel (a). Across the full range of target photon numbers, the success probability remains high, $P_{\text{succ}} \gtrsim 0.9$, indicating near-deterministic operation. (c) Photon-number distributions $P_n = \rho_{nn}$ in the Fock basis for the representative case $N = 100$ using a nine-pulse sequence ($p = 9$). Distributions are shown after the JC evolution of layers $k = 1, 4, 6$, and 9 (blue), and after the subsequent displacement operation (red). The progressive reshaping from a broad distribution into a sharply localized peak at the target photon number illustrates how displacement converts the engineered Fock-space interference into population localization. (d) Magnitude $|\rho_{nm}|$ of the reduced cavity density matrix after each JC evolution for the same four layers. Coherence is progressively concentrated into mirror-symmetric components, forming ridges along $n + m \simeq 2N$ that signal the emergence of a symmetric Fock-space wavepacket. (e) Corresponding phase maps $\arg(\rho_{nm})$. The phase structure evolves from an initial near-linear diagonal shear (layer 1) to strongly curved and ultimately anti-diagonal phase bands (layers 4 and 6), reflecting the nonlinear \sqrt{n} dispersion of the JC spectrum. By the final layer, well-defined phase alignment along $n + m = \text{const}$ enables the last displacement to induce constructive interference at $n = N$ and destructive interference elsewhere, yielding the target Fock state. For clarity, only matrix elements with sufficiently large magnitude are shown in the phase map of layer 9.

By the final layer, the displacement converts this engineered symmetry into selective destructive interference of all off-target components, yielding a sharply localized peak at the target photon number. The resulting Fock state exhibits the characteristic rich structure of Wigner negativities (see Fig. 1).

The generation dynamics underlying this redistribution is further elucidated in Figs. 2(d)–(e), which display the magnitude and phase of the JC-evolved density matrix for the same four layers. The magnitude maps $|\rho_{nm}|$ [Fig. 2(d)] reveal that coherence becomes progressively concentrated between Fock states symmetric with respect to the target photon number. In the later layers, the dominant matrix elements form ridges localized near $n + m \simeq 2N$, directly corresponding to the symmetric double-peak structure observed in the Fock-basis populations in Fig. 2(c). The corresponding phase maps $\arg(\rho_{nm})$ [Fig. 2(e)] show a systematic evolution from an initial linear diagonal phase gradient to curved and ultimately anti-diagonal phase bands, reflecting the nonlinear \sqrt{n} dispersion of the JC spectrum. By layer 9, the phase becomes approximately constant along lines $n + m = \text{const}$, indicating that mirror-related coherence elements acquire well-defined relative phases. This phase organization is crucial for the final

displacement, $\rho \rightarrow \hat{D}(\beta_9) \rho \hat{D}^\dagger(\beta_9)$, which mixes neighboring Fock components with phase-dependent weights. As a result, phase-aligned coherence along $n + m \simeq 2N$ interferes constructively at $n = N$ while canceling at all other photon numbers, yielding the desired Fock state.

D. Robustness analysis.

We now examine the robustness of the protocol against experimentally relevant imperfections, which can be broadly classified into two categories: (i) systematic control errors, including qubit–cavity detuning and inaccuracies in pulse timing and displacement amplitude, and (ii) environment-induced errors arising from open-system dynamics such as cavity photon loss and qubit spontaneous emission.

Detuning robustness. We first consider qubit–cavity detuning $\Delta = \omega_q - \omega_c$. The dependence of the post-selected fidelity on detuning is illustrated in the inset of Fig. 3(a) for a representative circuit depth $p = 10$. For small photon numbers ($N = 10$ and 20), the fidelity remains close to unity over a broad range of Δ/Ω , whereas for larger photon num-

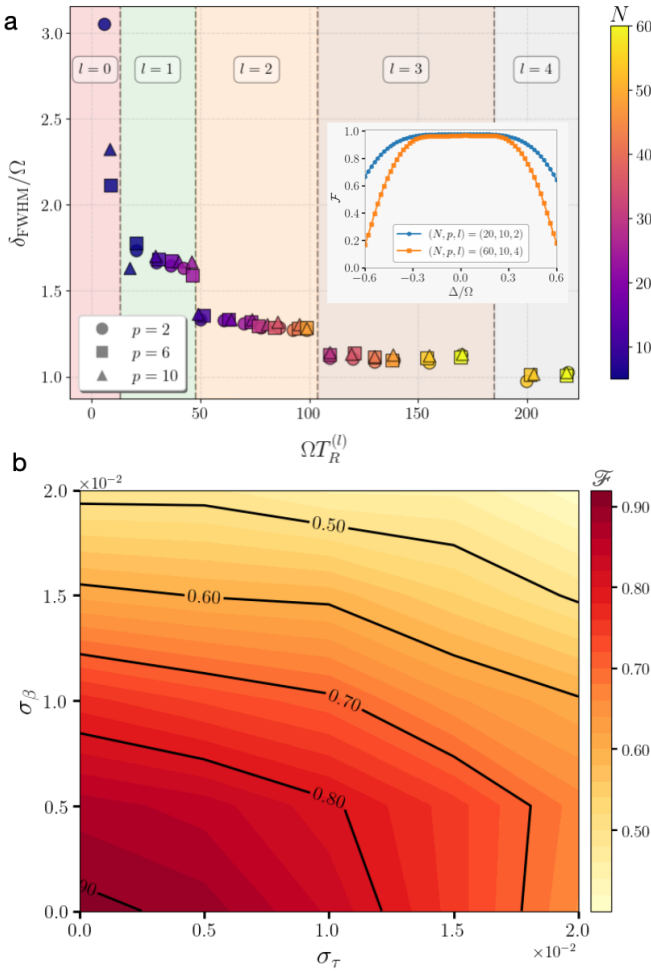


Figure 3. Robustness of the multi-pulse protocol against control noise and dissipation. (a) Post-selected fidelity as a function of qubit–cavity detuning Δ/Ω for representative target photon numbers. The inset highlights the fidelity response for a fixed circuit depth $p = 10$. (b) Average post-selected fidelity under pulse-timing and displacement errors for $N = 100$, $p = 9$, and $l = 5$. The control parameters are perturbed by independent Gaussian noise with standard deviations σ_τ and σ_β , and the fidelity is averaged over 200 noise realizations.

bers ($N = 60$) the high-fidelity plateau becomes noticeably narrower, reflecting the increased sensitivity of high- N Fock states to detuning-induced phase accumulation during the JC evolution. This behavior is quantified in Fig. 3(a), where the detuning tolerance is characterized by the full width at half maximum δ_{FWHM} as a function of the total evolution time $\Omega T_R^{(l)}$ for different circuit depths p . For small photon numbers or short total evolution times, δ_{FWHM} shows a clear dependence on the number of control layers: increasing p introduces additional phase structure and control complexity, which can reduce the effective detuning bandwidth. In contrast, for larger photon numbers the data for $p = 2, 6$, and 10 collapse onto a common trend, indicating a time-limited regime in which detuning-induced phase errors are governed primarily by the total accumulated interaction time, rather

than by the specific segmentation of the sequence. Importantly, the extracted detuning half-widths remain on the order of, or larger than, the qubit–cavity coupling strength Ω , indicating that the protocol does not rely on fine frequency matching.

Pulse errors. We next analyze the impact of control inaccuracies in the JC evolution times and displacement amplitudes. The implemented control parameters are modeled as

$$\tau_k = \tau_k^* + \xi_k^\tau, \quad \beta_k = \beta_k^* + \xi_k^\beta, \quad (6)$$

where the noise variables ξ_k^τ and the real and imaginary parts of ξ_k^β are sampled independently from zero-mean Gaussian distributions with variances σ_τ^2 and σ_β^2 , respectively.

Figure 3(b) summarizes the resulting fidelity landscape for a representative large-photon-number case with $(N, p, l) = (100, 9, 5)$. Each data point corresponds to the post-selected fidelity averaged over 200 independent realizations of the control noise. For qubit–cavity coupling strengths in the range $\Omega/2\pi \sim \text{kHz–MHz}$, typical of current cavity or circuit QED platforms, the total evolution time T_N spans from several tens of milliseconds down to the sub-millisecond regime. Each JC segment therefore has a characteristic duration $\tau_k \sim T_N/p$, placing it in the sub-millisecond to millisecond range across these platforms. In practical AMO experiments [56], the evolution time of a gate operation is typically controlled by an arbitrary waveform generator with sampling rates reaching the gigahertz regime, enabling temporal accuracy at the level of a few tens of nanoseconds. Comparing these timescales indicates that relative timing errors can be well controlled below the percent level under realistic experimental conditions [58]. The displacement amplitudes can be calibrated with reliable experimental control and stability [11, 16, 50, 59].

Dissipation effects. We finally assess the performance of the multi-pulse protocol in the presence of open-system dynamics arising from cavity photon loss and atomic spontaneous emission. The system evolution is modeled by the Lindblad master equation

$$\dot{\rho}(t) = -i[\hat{H}, \rho(t)] + \frac{\kappa}{2}\mathcal{D}[\hat{a}]\rho + \frac{\Gamma}{2}\mathcal{D}[\hat{\sigma}_-]\rho, \quad (7)$$

where κ and Γ denote the cavity decay and atomic spontaneous emission rates, respectively, and $\mathcal{D}[\hat{o}]\rho = 2\hat{o}\rho\hat{o}^\dagger - \hat{o}\hat{o}^\dagger\rho - \rho\hat{o}\hat{o}^\dagger$ is the Lindblad superoperator. Rather than performing an exhaustive parameter scan, we provide here an experimentally grounded estimate based on realistic parameters.

A particularly promising experimental platform is provided by atom-array cavity QED, where two-dimensional ordered atomic arrays in free space form an effective optical cavity with well-defined cavity-QED parameters. For the ^{87}Rb D-line, Ref. [60] estimates a spontaneous emission rate $\Gamma \simeq 2\pi \times 6 \text{ MHz}$ and an effective cavity loss rate $\kappa \simeq 2\pi \times 0.06 \text{ MHz}$ in a motion-limited lattice configuration, while demonstrating that optimized atomic placement can reach cooperativities as large as $C \gtrsim 10^4$. These parameters correspond to a deep strong-coupling regime, in which cavity loss and spontaneous emission act as weak perturbations to the coherent light–matter dynamics.

Using these experimentally motivated values, and starting from a unitary-optimized fidelity exceeding $\mathcal{F}(N = 100) \gtrsim 0.93$, we find that the inclusion of dissipation leads only to a moderate reduction of the final state fidelity. In particular, for cooperativities in the $C \sim 10^4$ range, the accumulated effect of cavity decay and spontaneous emission over the full multi-pulse sequence remains compatible with a final fidelity $\gtrsim 0.8$. This demonstrates that the deterministic preparation of large Fock states with $N = 100$ is feasible under realistic dissipation.

Importantly, these constraints can be further relaxed by exploiting collective light-matter coupling in atomic ensembles [52, 60–63]. In this case, the effective coupling is enhanced as $\Omega_{\text{eff}} = \Omega\sqrt{N_{\text{atom}}}$ due to symmetric collective states in the single-excitation manifold [64]. This collective enhancement is fully compatible with the atom-array cavity architecture and effectively shortens the required coherent evolution time, thereby providing an additional suppression of dissipative effects. Together with the robustness of the multi-pulse control, these considerations indicate that deterministic, high-fidelity preparation of Fock states well beyond $N = 100$ is a realistic prospect in state-of-the-art AMO platforms.

III. DISCUSSION

In this work, we introduced a multi-pulse Jaynes–Cummings–displacement protocol for scalable generation of large photonic Fock states. By alternating Jaynes–Cummings evolutions with phase-space displacements, the protocol engineers photon-number-dependent phases and converts them into selective interference in Fock space, yielding high-fidelity

preparation of $|N\rangle$ with $\mathcal{F} \gtrsim 0.9$ up to $N \gtrsim 100$ using shallow control depths. An optional qubit projection further removes residual qubit–field correlations with near-unity success probability.

Our results provide an experimentally accessible route to large- N Fock state preparation using only native qubit–oscillator operations, applicable to cavity and circuit QED, trapped ions, and related AMO platforms. Looking forward, the same interference-engineering approach can be extended to prepare more general nonclassical bosonic resources, such as Fock-state superpositions and grid-like states, and to optimize probe states for quantum-enhanced sensing. In addition, incorporating platform-specific constraints and dissipation into the optimization loop offers a practical pathway toward hardware-ready pulse sequences and further scaling to larger photon numbers.

Note added. During the preparation of this manuscript, we became aware of a closely related preprint that introduces a similar Fock-space interference approach based on Kerr-induced nonlinear phase modulation for generating macroscopic Fock states [65].

Acknowledgement We thank Dr. Mariano Uria for providing data and helpful discussions related to the single-pulse case. This work was supported by the National Natural Science Foundation of China (Grant No. 12304543), the Innovation Program for Quantum Science and Technology (Grant No. 2021ZD0302100), the Natural Science Foundation of Jiangsu Province (Grant No. SBK20250403716), the Frontier Technology Research Program of Suzhou (Grant No. SYG202322), and the Youth Science and Technology Talent Support Project of Jiangsu Province.

[1] S. L. Braunstein and P. van Loock, Quantum information with continuous variables, *Rev. Mod. Phys.* **77**, 513 (2005).

[2] J. Loredo, M. Broome, P. Hilaire, O. Gazzano, I. Sagnes, A. Lemaitre, M. Almeida, P. Senellart, and A. White, Boson sampling with single-photon fock states from a bright solid-state source, *Phys. Rev. Lett.* **118**, 130503 (2017).

[3] H. Wang, Y. He, Y.-H. Li, Z.-E. Su, B. Li, H.-L. Huang, X. Ding, M.-C. Chen, C. Liu, J. Qin, *et al.*, High-efficiency multiphoton boson sampling, *Nature Photonics* **11**, 361 (2017).

[4] F. Wolf, C. Shi, J. C. Heip, M. Gessner, L. Pezzè, A. Smerzi, M. Schulte, K. Hammerer, and P. O. Schmidt, Motional fock states for quantum-enhanced amplitude and phase measurements with trapped ions, *Nature Communications* **10**, 2929 (2019).

[5] D. Gottesman, A. Kitaev, and J. Preskill, Encoding a qubit in an oscillator, *Phys. Rev. A* **64**, 012310 (2001).

[6] M. Walschaers, Non-gaussian quantum states and where to find them, *PRX Quantum* **2**, 030204 (2021).

[7] J. Deng, H. Dong, C. Zhang, Y. Wu, J. Yuan, X. Zhu, F. Jin, H. Li, Z. Wang, H. Cai, *et al.*, Observing the quantum topology of light, *Science* **378**, 966 (2022).

[8] M. S. Winnel, J. J. Guanzon, D. Singh, and T. C. Ralph, Deterministic preparation of optical squeezed cat and gottesman–kitaev–preskill states, *Phys. Rev. Lett.* **132**, 230602 (2024).

[9] A. L. Grimsmo and S. Puri, Quantum error correction with the gottesman–kitaev–preskill code, *PRX Quantum* **2**, 020101 (2021).

[10] A. Blais, S. M. Girvin, and W. D. Oliver, Quantum information processing and quantum optics with circuit quantum electrodynamics, *Nat. Phys.* **16**, 247 (2020).

[11] D. Hoshi, T. Nagase, S. Kwon, D. Iyama, T. Kamiya, S. Fujii, H. Mukai, S. Ahmed, A. F. Kockum, S. Watabe, *et al.*, Entangling schrödinger’s cat states by bridging discrete- and continuous-variable encoding, *Nature communications* **16**, 1309 (2025).

[12] P. T. Grochowski and R. Filip, Optimal phase-insensitive force sensing with non-gaussian states, *Phys. Rev. Lett.* **135**, 230802 (2025).

[13] T. J. Sturges, T. McDermott, A. Buraczewski, W. R. Clements, J. J. Renema, S. W. Nam, T. Gerrits, A. Lita, W. S. Kolthammer, A. Eckstein, I. A. Walmsley, and M. Stobińska, Quantum simulations with multiphoton fock states, *npj Quantum Information* **7**, 91 (2021).

[14] C. Couteau, S. Barz, T. Durt, T. Gerrits, J. Huwer, R. Prevedel, J. Rarity, A. Shields, and G. Weihs, Applications of single photons in quantum metrology, biology and the foundations of quantum physics, *Nat. Rev. Phys.* **5**, 354 (2023).

[15] M. Perarnau-Llobet, A. González-Tudela, and J. I. Cirac, Multimode fock states with large photon number: effective descriptions and applications in quantum metrology, *Quantum Science and Technology* **5**, 025003 (2020).

[16] X. Deng, S. Li, Z.-J. Chen, Z. Ni, Y. Cai, J. Mai, L. Zhang, P. Zheng, H. Yu, C.-L. Zou, S. Liu, F. Yan, Y. Xu, and D. Yu, Quantum-enhanced metrology with large Fock states, *Nature Physics* [10.1038/s41567-024-02619-5](https://doi.org/10.1038/s41567-024-02619-5) (2024).

[17] H.-S. Zhong, H. Wang, Y.-H. Deng, M.-C. Chen, L.-C. Peng, Y.-H. Luo, J. Qin, D. Wu, X. Ding, Y. Hu, *et al.*, Quantum computational advantage using photons, *Science* **370**, 1460 (2020).

[18] L. S. Madsen, F. Laudenbach, M. F. Askarani, F. Rortais, T. Vincent, J. F. Bulmer, F. M. Miatto, L. Neuhaus, L. G. Helt, M. J. Collins, *et al.*, Quantum computational advantage with a programmable photonic processor, *Nature* **606**, 75 (2022).

[19] A. D. O'Connell, M. Hofheinz, M. Ansmann, R. C. Bialczak, M. Lenander, E. Lucero, M. Neeley, D. Sank, H. Wang, M. Weides, *et al.*, Quantum ground state and single-phonon control of a mechanical resonator, *Nature* **464**, 697 (2010).

[20] I. Aharonovich, D. Englund, and M. Toth, Solid-state single-photon emitters, *Nat. Photonics* **10**, 631 (2016).

[21] S. P. Premaratne, F. Wellstood, and B. Palmer, Microwave photon fock state generation by stimulated raman adiabatic passage, *Nature Communications* **8**, 14148 (2017).

[22] W. Wang, L. Hu, Y. Xu, K. Liu, Y. Ma, S.-B. Zheng, R. Vijay, Y. P. Song, L.-M. Duan, and L. Sun, Converting quasiclassical states into arbitrary fock state superpositions in a superconducting circuit, *Phys. Rev. Lett.* **118**, 223604 (2017).

[23] A. Migdall, S. V. Polyakov, J. Fan, and J. C. Bienfang, *Single-photon generation and detection: physics and applications* (Academic Press, 2013).

[24] R. Uppu, F. T. Pedersen, Y. Wang, C. T. Olesen, C. Papon, X. Zhou, L. Midolo, S. Scholz, A. D. Wieck, A. Ludwig, *et al.*, Scalable integrated single-photon source, *Sci. Adv.* **6**, eabc8268 (2020).

[25] G. P. Teja, C. Kumar, L. c. v. Lachman, and R. Filip, Quantum non-gaussian high fock states of light pulses and their superpositions, *Phys. Rev. Res.* **7**, 033272 (2025).

[26] Q. R. Rahman, I. Kladarić, M.-E. Kern, L. c. v. Lachman, Y. Chu, R. Filip, and M. Fadel, Genuine quantum non-gaussianity and metrological sensitivity of fock states prepared in a mechanical resonator, *Phys. Rev. Lett.* **134**, 180801 (2025).

[27] M. Hofheinz, E. Weig, M. Ansmann, R. C. Bialczak, E. Lucero, M. Neeley, A. O'connell, H. Wang, J. M. Martinis, and A. Cleland, Generation of fock states in a superconducting quantum circuit, *Nature* **454**, 310 (2008).

[28] H. Wang, M. Hofheinz, M. Ansmann, R. Bialczak, E. Lucero, M. Neeley, A. O'connell, D. Sank, J. Wenner, A. Cleland, *et al.*, Measurement of the decay of fock states in a superconducting quantum circuit, *Phys. Rev. Lett.* **101**, 240401 (2008).

[29] M. Hofheinz, H. Wang, M. Ansmann, R. C. Bialczak, E. Lucero, M. Neeley, A. O'connell, D. Sank, J. Wenner, J. M. Martinis, *et al.*, Synthesizing arbitrary quantum states in a superconducting resonator, *Nature* **459**, 546 (2009).

[30] P. Bertet, A. Auffeves, P. Maioli, S. Osnaghi, T. Meunier, M. Brune, J. M. Raimond, and S. Haroche, Direct measurement of the wigner function of a one-photon fock state in a cavity, *Phys. Rev. Lett.* **89**, 200402 (2002).

[31] A. M. Brańczyk, T. Ralph, W. Helwig, and C. Silberhorn, Optimized generation of heralded fock states using parametric down-conversion, *New J. Phys.* **12**, 063001 (2010).

[32] J. Tiedau, T. J. Bartley, G. Harder, A. E. Lita, S. W. Nam, T. Gerrits, and C. Silberhorn, Scalability of parametric down-conversion for generating higher-order fock states, *Phys. Rev. A* **100**, 041802 (2019).

[33] X.-D. Zhou, S. Wang, H. Zhang, T.-B. Zhang, Y.-H. Chen, W. Qin, Y. Ning, and Y. Xia, Fast generation of 2n-photon fock states using shortcuts to adiabaticity and ultrastrong light-matter coupling, *Annalen der Physik* **535**, 2200348 (2023).

[34] C. Sayrin, I. Dotsenko, X. Zhou, B. Peaudecerf, T. Rybarczyk, S. Gleyzes, P. Rouchon, M. Mirrahimi, H. Amini, M. Brune, *et al.*, Real-time quantum feedback prepares and stabilizes photon number states, *Nature* **477**, 73 (2011).

[35] X. Zhou, I. Dotsenko, B. Peaudecerf, T. Rybarczyk, C. Sayrin, S. Gleyzes, J. Raimond, M. Brune, and S. Haroche, Field locked to a fock state by quantum feedback with single photon corrections, *Physical review letters* **108**, 243602 (2012).

[36] B. Peaudecerf, C. Sayrin, X. Zhou, T. Rybarczyk, S. Gleyzes, I. Dotsenko, J. Raimond, M. Brune, and S. Haroche, Quantum feedback experiments stabilizing fock states of light in a cavity, *Phys. Rev. A* **87**, 042320 (2013).

[37] M. Uria, P. Solano, and C. Hermann-Avigliano, Deterministic generation of large fock states, *Phys. Rev. Lett.* **125**, 093603 (2020).

[38] V. Sivak, A. Eickbusch, H. Liu, B. Royer, I. Tsoutsios, and M. Devoret, Model-free quantum control with reinforcement learning, *Phys. Rev. X* **12**, 011059 (2022).

[39] G. Teja and Chanchal, Distillation of optical fock states using atom-cavity systems, *Phys. Rev. Appl.* **20**, 044049 (2023).

[40] C.-y. Zhang and J. Jing, Generating fock-state superpositions from coherent states by selective measurement, *Phys. Rev. A* **110**, 042421 (2024).

[41] T. Fösel, S. Krastanov, F. Marquardt, and L. Jiang, Efficient cavity control with snap gates, *arXiv preprint arXiv:2004.14256* (2020).

[42] R. Yanagimoto, E. Ng, T. Onodera, and H. Mabuchi, Adiabatic fock-state-generation scheme using kerr nonlinearity, *Phys. Rev. A* **100**, 033822 (2019).

[43] A. Lingenfelter, D. Roberts, and A. Clerk, Unconditional fock state generation using arbitrarily weak photonic nonlinearities, *Sci. Adv.* **7**, eabj1916 (2021).

[44] N. Rivera, J. Sloan, Y. Salamin, J. D. Joannopoulos, and M. Soljačić, Creating large fock states and massively squeezed states in optics using systems with nonlinear bound states in the continuum, *PNAS* **120**, e2219208120 (2023).

[45] S. Li, Z. Ni, L. Zhang, Y. Cai, J. Mai, S. Wen, P. Zheng, X. Deng, S. Liu, Y. Xu, and D. Yu, Autonomous stabilization of fock states in an oscillator against multiphoton losses, *Phys. Rev. Lett.* **132**, 203602 (2024).

[46] J. Fink, M. Göppl, M. Baur, R. Bianchetti, P. J. Leek, A. Blais, and A. Wallraff, Climbing the jaynes-cummings ladder and observing its nonlinearity in a cavity qed system, *Nature* **454**, 315 (2008).

[47] M. M. Lund, F. Yang, V. R. Christiansen, D. Kornovan, and K. Mølmer, Subtraction and addition of propagating photons by two-level emitters, *Phys. Rev. Lett.* **133**, 103601 (2024).

[48] A. Pasharavesh and M. Bajcsy, Multi-photon fock state generation via selective single photon subtraction in a cascaded waveguide qed system, *Advanced Quantum Technologies* **1**, 2400616 (2025).

[49] R. W. Heeres, B. Vlastakis, E. Holland, S. Krastanov, V. V. Albert, L. Frunzio, L. Jiang, and R. J. Schoelkopf, Cavity state manipulation using photon-number selective phase gates, *Phys. Rev. Lett.* **115**, 137002 (2015).

[50] A. Eickbusch, V. Sivak, A. Z. Ding, S. S. Elder, S. R. Jha, J. Venkatraman, B. Royer, S. M. Girvin, R. J. Schoelkopf, and M. H. Devoret, Fast universal control of an oscillator with weak dispersive coupling to a qubit, *Nat. Phys.* **18**, 1464 (2022).

[51] J. Landgraf, C. Flühmann, T. Fösel, F. Marquardt, and R. J. Schoelkopf, Fast quantum control of cavities using an improved protocol without coherent errors, *Phys. Rev. Lett.* **133**, 260802 (2024).

[52] F. Mivehvar, F. Piazza, T. Donner, and H. Ritsch, Cavity qed with quantum gases: New paradigms in many-body physics, *Advances in Physics* **70**, 1 (2021).

[53] A. Blais, A. L. Grimsmo, S. M. Girvin, and A. Wallraff, Circuit quantum electrodynamics, *Rev. Mod. Phys.* **93**, 025005 (2021).

[54] Y. Wu and X. Yang, Jaynes-cummings model for a trapped ion in any position of a standing wave, *Physical review letters* **78**, 3086 (1997).

[55] D. Leibfried, R. Blatt, C. Monroe, and D. Wineland, Quantum dynamics of single trapped ions, *Reviews of Modern Physics* **75**, 281 (2003).

[56] J. Ye and P. Zoller, Essay: Quantum sensing with atomic, molecular, and optical platforms for fundamental physics, *Phys. Rev. Lett.* **132**, 190001 (2024).

[57] R. Robinett, Quantum wave packet revivals, *Physics Reports* **392**, 1 (2004).

[58] L. Sun, A. Petrenko, Z. Leghtas, B. Vlastakis, G. Kirchmair, K. Sliwa, A. Narla, M. Hatridge, S. Shankar, J. Blumoff, *et al.*, Tracking photon jumps with repeated quantum non-demolition parity measurements, *Nature* **511**, 444 (2014).

[59] L. D. Burkhardt, J. D. Teoh, Y. Zhang, C. J. Axline, L. Frunzio, M. Devoret, L. Jiang, S. Girvin, and R. Schoelkopf, Error-detected state transfer and entanglement in a superconducting quantum network, *PRX Quantum* **2**, 030321 (2021).

[60] D. Castells-Graells, J. I. Cirac, and D. S. Wild, Cavity quantum electrodynamics with atom arrays in free space, *Phys. Rev. A* **111**, 053712 (2025).

[61] Y. Liu, Z. Wang, P. Yang, Q. Wang, Q. Fan, S. Guan, G. Li, P. Zhang, and T. Zhang, Realization of strong coupling between deterministic single-atom arrays and a high-finesse miniature optical cavity, *Phys. Rev. Lett.* **130**, 173601 (2023).

[62] R. Pennetta, D. Lechner, M. Blaha, A. Rauschenbeutel, P. Schneeweiss, and J. Volz, Observation of coherent coupling between super-and subradiant states of an ensemble of cold atoms collectively coupled to a single propagating optical mode, *Physical Review Letters* **128**, 203601 (2022).

[63] M. Blaha, A. Johnson, A. Rauschenbeutel, and J. Volz, Beyond the tavis-cummings model: Revisiting cavity qed with ensembles of quantum emitters, *Phys. Rev. A* **105**, 013719 (2022).

[64] M. Fleischhauer and M. D. Lukin, Quantum memory for photons: Dark-state polaritons, *Phys. Rev. A* **65**, 022314 (2002).

[65] M. Li, W. Cai, Z. Hua, Y. Xu, Y. Zhou, Z.-J. Chen, X.-B. Zou, G.-C. Guo, L. Sun, and C.-L. Zou, Scalable generation of macroscopic fock states exceeding 10,000 photons, arXiv preprint arXiv:2601.05118 (2026).